Journal of Power Sources 228 (2013) 214–219

Contents lists available at SciVerse ScienceDirect

Journal of Power Sources

journal homepage: www.elsevier.com/locate/jpowsour

Short communication

Novel precursor of $Mn(PO_3(OH))\cdot 3H_2O$ for synthesizing $LiMn_{0.5}Fe_{0.5}PO_4$ cathode material

Jun Zong [a], Qingwen Peng [b], Jinpeng Yu [b], Xingjiang Liu [a,b,*]

[a] Department of Applied Chemistry, School of Chemical Engineering and Technology, Tianjin University, Tianjin 300072, PR China
[b] National Key Lab of Power Sources, Tianjin Institute of Power Sources, Tianjin 300384, PR China

HIGHLIGHTS

- Pure $Mn(PO_3(OH))\cdot 3H_2O$ was successfully prepared using C_2H_5OH for the first time.
- The process for synthesizing $Mn(PO_3(OH))\cdot 3H_2O$ is easy and low-cost.
- $LiMnPO_4$ and $LiMn_{0.5}Fe_{0.5}PO_4$ were first prepared via the $Mn(PO_3(OH))\cdot 3H_2O$ precursor.
- The $LiMn_{0.5}Fe_{0.5}PO_4$/C material exhibited a good reversible capacity.

ARTICLE INFO

Article history:
Received 16 July 2012
Received in revised form
29 September 2012
Accepted 12 November 2012
Available online 29 November 2012

Keywords:
Precipitation
Olivine-structure
Cathode material
Lithium ion battery

ABSTRACT

A brand new method for synthesizing $Mn(PO_3(OH))\cdot 3H_2O$ is attained in this paper. During this process, pure flake-like $Mn(PO_3(OH))\cdot 3H_2O$ precipitate is prepared using C_2H_5OH as initiator. Besides that, $LiMn_{0.5}Fe_{0.5}PO_4$/C is successfully synthesized from the $Mn(PO_3(OH))\cdot 3H_2O$ precursor at 650 °C for the first time. Thermogravimetric analysis (TGA), X-ray diffraction (XRD) and scanning electron microscopy (SEM) are applied in the characterization of the $Mn(PO_3(OH))\cdot 3H_2O$ precursor and $LiMn_{0.5}Fe_{0.5}PO_4$/C. High-resolution transmission electron microscopy (HRTEM) is also used to investigate the morphology of $LiMn_{0.5}Fe_{0.5}PO_4$/C. X-ray photoelectron spectroscopy (XPS) and galvanostatic charge and discharge test are employed to characterize the $Mn(PO_3(OH))\cdot 3H_2O$ precursor and $LiMn_{0.5}Fe_{0.5}PO_4$ material, respectively. The as-prepared $LiMn_{0.5}Fe_{0.5}PO_4$/C material exhibited a reversible capacity of 131 mAh g^{-1} at 0.05 C. It can be confirmed that the incorporation of Fe into $LiMnPO_4$ can significantly improve the electrochemical properties for improving the conductivity of the material and facilitating the Li^+ diffusion. In addition, a capacity of 120 mAh g^{-1} is still delivered at 0.05 C rate with a capacity retention of about 91% after 25 cycles, and reversible capacity can reach 105 mAh g^{-1} at 1 C.

1. Introduction

Precursor-based method has been widely applied in synthesizing different materials, such as, high dielectric constant material [1], optoelectronic material [2], magnetic material [3], and semiconducting material [4], etc. And this method can be understood as follows: i) preparing appropriate precursors, ii) treating the acquired precursors to get the terminal materials. So the precursors play an important role in the precursor-based method, and therefore, seeking for low-cost and easy accessible method for preparing novel precursor is now recognized as one of the tasks for materials research. Especially, precursor-based method is an excellent method for synthesizing cathode materials of Lithium ion batteries.

As for cathode materials, olivine-structured $LiMPO_4$ (M = Mn, Fe, Ni, etc.) materials have attracted great much attention due to many advantages such as lower toxicity, lower cost, better thermal and chemical stability [5–7]. On that basis, researchers have paid much attention on Mn–P precursors (precursors that contain Mn and P elements) for preparing $LiMnPO_4$ due to the following unique advantages [8–11]: i) it can significantly reduce the common impurities (such as Li_3PO_4) produced during the reaction. ii) the morphology and size distribution of the precursor can be preserved at a certain extent, so the terminal material can be controlled through regulating the precursor. iii) this cost-effective method is appropriate for the mass production of $LiMPO_4$ material. In their work, the common Mn–P precursors are $NH_4MnPO_4\cdot H_2O$ and

* Corresponding author. National Key Lab of Power Sources, Tianjin Institute of Power Sources, Tianjin 300384, PR China. Tel.: +86 2223959300; fax: +86 2223383783.
E-mail address: xjliu@nklps.org (X. Liu).

0378-7753/$ – see front matter © 2012 Published by Elsevier B.V.
http://dx.doi.org/10.1016/j.jpowsour.2012.11.103

$MnPO_4 \cdot H_2O$. Unfortunately, these Mn–P precursors have not been used to attain $LiMn_{0.5}Fe_{0.5}PO_4$ material which has better electrochemical performance than that of $LiMnPO_4$ material because the Fe substitution may improve the kinetics during the charge/discharge process [12,13]. Balaya et al. [14] reported that the $LiMn_{0.5}Fe_{0.5}PO_4$ material was successfully prepared through hydrothermal reaction. And then, Sun et al. [15] used $Mn_{0.5}Fe_{0.5}PO_4$ precursor to synthesize $LiMn_{0.5}Fe_{0.5}PO_4$ with an excellent reversible capacity of 140 mAh g^{-1} at 0.05 C (at 25 °C). Besides that, $LiMn_{0.5}Fe_{0.5}PO_4$ was also attained though sol–gel process by other researchers [16].

In this paper, we introduced an easy accessible method for preparing $Mn(PO_3(OH)) \cdot 3H_2O$ and used it as a novel Mn–P precursor to get the $LiMn_{0.5}Fe_{0.5}PO_4$ material for the first time. The crystal of $Mn(PO_3(OH)) \cdot 3H_2O$ was first prepared by Cudennec et al. [17] in 1989. After that, Sharma et al. [18] got the crystal using both solvent evaporation and hydrothermal techniques and studied on the magnetic property of this material. And then, Larrañaga et al. [19] successfully prepared $Mn(PO_3(OH)) \cdot 3H_2O$ by adjusting pH value (pH = 6) and had structural, luminescent and magnetic studies on the compound. But no one attempted to use it as precursor to attain $LiMnPO_4$ material. During our synthesis process, $Mn(PO_3(OH)) \cdot 3H_2O$ precipitated from the solution using anhydrous ethanol as initiator. And $LiMn_{0.5}Fe_{0.5}PO_4$/C was successfully synthesized by solid-state reaction from this novel precursor. It paves a promising way of simplicity and low cost to obtain the $LiMn_{0.5}Fe_{0.5}PO_4$/C solid-solution with improved electrochemical performance.

2. Experimental

To prepare $Mn(PO_3(OH)) \cdot 3H_2O$, $MnSO_4 \cdot H_2O$ (0.06 mol) and $NH_4H_2PO_4$ (0.06 mol) was stirred into 420 mL de-ionized water (DI) at room temperature (25 °C) firstly. Then anhydrous ethanol (200 mL) was added into the solution by drop-wise (1 ~ 2d s^{-1}). After that, maintained agitation for 4.5 h and filtered the final suspension to get the white precipitation ($Mn(PO_3(OH)) \cdot 3H_2O$). The acquired product was washed with de-ionized water for 3–4 times and dried at 60 °C for 18 h.

For synthesizing $LiMn_{0.5}Fe_{0.5}PO_4$, $Mn(PO_3(OH)) \cdot 3H_2O$ was ball-milled with a stoichiometric amount of $LiAc \cdot 2H_2O$, $FeCl_2 \cdot 4H_2O$, $NH_4H_2PO_4$ and a certain amount of sucrose and acetylene black (generate 30 wt.% carbon in the final product) for 6 h. The mixture was then pre-sintered at 350 °C for 4 h in N_2/H_2 (92% N_2 + 8% H_2) atmosphere; and the pre-sintered product was then was ball-milled 6 h; then further calcined at 650 °C for 12 h in N_2/H_2 (92% N_2 + 8% H_2) atmosphere to get $LiMn_{0.5}Fe_{0.5}PO_4$. For comparison, $LiMnPO_4$ was prepared from the same route.

The crystalline structure of $Mn(PO_3(OH)) \cdot 3H_2O$ and $LiMn_{0.5}Fe_{0.5}PO_4$ were determined by X-ray diffraction (XRD, D/max 2400 V, Rigaku, Japan) with Cu-Kα irradiation. The morphology of the samples was observed using scanning electron microscope (SEM, S4800, Hitachi, Japan) and high-resolution transmission electron microscopy (HRTEM, tecnai G2 F20). A combined differential scanning calorimetry/thermogravimetric analysis (DSC/TGA) instrument (Netzsch, STA 449C) was employed to study the decomposition and reaction of the precursor. The powder sample of $Mn(PO_3(OH)) \cdot 3H_2O$ was heated in an N_2 environment to 800 °C at a ramp rate of 5 °C min^{-1}. X-ray photoelectron spectroscopy (PHI 1600 XPS spectrometer, USA) was used to characterize the $Mn(PO_3(OH)) \cdot 3H_2O$. And the XPS spectra were recorded with Mg Kα radiation as an excitation source.

The 2430 coin-type cells were employed to test the electrochemical performances of acquired materials. The cathode electrodes were fabricated by mixing the active materials, acetylene black and polyvinylidene fluoride (PVDF) with a mass ratio of 80:10:10, the anode was metallic lithium foil, the electrolyte was 1.0 M $LiPF_6$ in ethylene carbonate and dimethyl carbonate with a volumetric ratio of 1:1. LAND-CT2001A battery cycler (Wuhan, China) was used to evaluate the charge/discharge performances in a potential range of 2.2–4.5 V (vs. Li/Li^+) at 25 °C.

3. Results and discussion

Fig. 1 shows the XRD pattern of as-prepared $Mn(PO_3(OH)) \cdot 3H_2O$. Compared with the PDF card, all the diffraction peaks are fully indexed as pure $Mn(PO_3(OH)) \cdot 3H_2O$. As shown in Fig. 1, the relative intensity of the peaks is slightly different from the standard ones, implying that it may preferentially grow along (020) orientation. Besides that, all reflections can be indexed based on the orthorhombic unit cell *Pbca*. The lattice parameters was calculated to be a = 10.3966(7) Å, b = 10.8712(1) Å and c = 10.1832(7) Å by refining the XRD pattern. And the crystal structure of $Mn(PO_3(OH)) \cdot 3H_2O$ is shown in the inset [18] (Fig. 1). The octahedra and tetrahedra represent the $MnO_6(H_6)$ and $PO_4(H)$ coordination, in other words, Mn is coordinated by three H_2O molecules and three oxygen atoms of HPO_4. Unlike the structure of $LiMnPO_4$, they ($MnO_6(H_6)$ and $PO_4(H)$) share corners but no edge.

The TG/DSC curves of the $Mn(PO_3(OH)) \cdot 3H_2O$ precursor are shown in Fig. 2. The DSC curve shows two peaks whose positions are around 98.7 °C and 572.3 °C, respectively. After combining these peak positions with the TG curve, it can be confirmed that main mass loss lies between 65 °C and 600 °C. And the weight loss of the precursor is about 30.7% according to the TG curve. As Sharma et al. [18] reported, the precursor may undergo the dehydration process, but the concrete reaction equation was not given. To obtain an accurate reaction equation, the $Mn(PO_3(OH)) \cdot 3H_2O$ precursor was calcined at 650 °C for 5 h in flowing ultra-pure N_2/H_2 and the product was subsequently characterized by XRD. As shown in Fig. 3, all the diffraction peaks in the pattern are in agreement with those of $Mn_2P_2O_7$ (PDF#29–0891). So the thermal decomposition reaction of the precursor can be considered as follows:

$$Mn(PO_3(OH)) \cdot 3H_2O \rightarrow 1/2\ Mn_2P_2O_7 + 7/2\ H_2O \quad (1)$$

Therefore the theoretical weight loss is absolutely 30.74%, which is consistent with the result of the TG curve. Based on above analysis, it can be confirmed that the as-prepared sample is

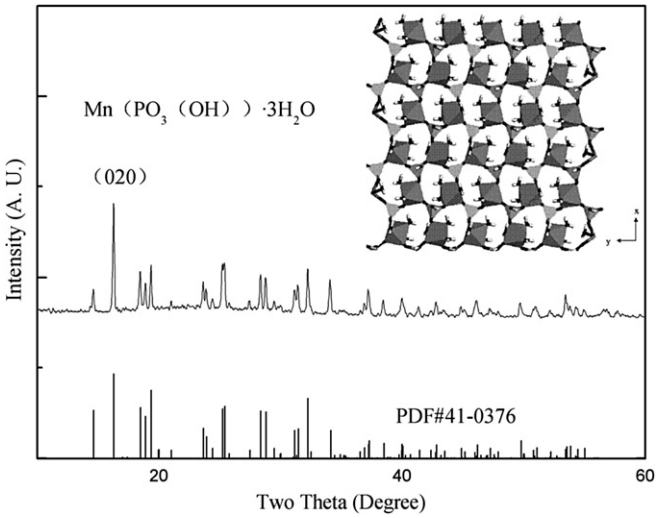

Fig. 1. XRD pattern of as-prepared $Mn(PO_3(OH)) \cdot 3H_2O$ with Cu-Kα irradiation.

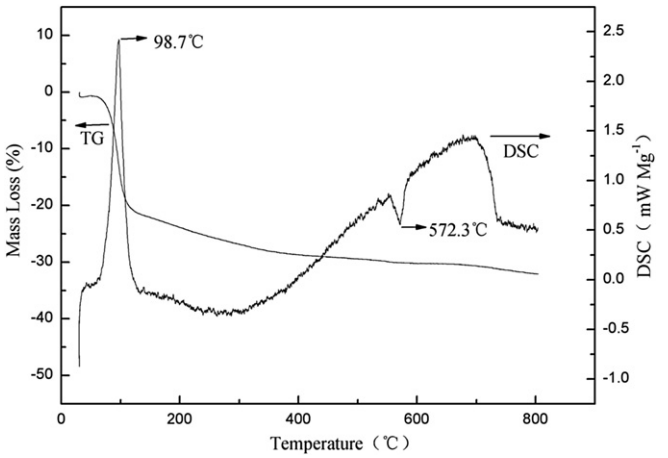

Fig. 2. TG/DSC curves of $Mn(PO_3(OH))\cdot 3H_2O$ precursor in N_2 at a ramp rate of 5 °C min^{-1}.

absolutely pure $Mn(PO_3(OH))\cdot 3H_2O$ and the easy accessible method for preparing $Mn(PO_3(OH))\cdot 3H_2O$ is successful.

$$Mn^{2+} + H_2PO_4^- + 3H_2O \rightarrow Mn(PO_3(OH))\cdot 3H_2O + H^+ \quad (2)$$

During the synthesis process of the precursor, the reactions may take place as equation (2).After stirring $MnSO_4\cdot H_2O$ and $NH_4H_2PO_4$ into the DI water, Mn^{2+} and $H_2PO_4^-$ will exist in the solution. And the $H_2PO_4^-$ has equilibrium reactions which is shown in equation (3) [20].

$$H_2PO_4^- \rightleftharpoons H^+ + HPO_4^{2-} \rightleftharpoons H^+ + PO_4^{3-} \quad (3)$$

The anhydrous ethanol added into the solution might break the equilibrium and facilitate the formation of HPO_4^{2-}. Thus the pH value of the solution would be less than 7, but the acidity was very weak. In these conditions, $MnHPO_4$ can precipitate from the solution [18,20]. For these reasons, the acquired HPO_4^{2-} might combine with Mn^{2+}/H_2O to form precipitate. As the standard XRD patterns shown (PDF#41-0376 and PDF#25–0541), all peak positions of $Mn(PO_3(OH))\cdot 3H_2O$ are the same as those of $MnHPO_4\cdot 3H_2O$, but their relative intensities of the peaks are different. Therefore, in the precipitation process, it may preferentially form the crystal of $Mn(PO_3(OH))\cdot 3H_2O$ instead of $MnHPO_4\cdot 3H_2O$ due to the existence of anhydrous ethanol in the solution. The concrete mechanism of the reactions has not been attained.

From the SEM image (Fig. 4) of $Mn(PO_3(OH))\cdot 3H_2O$, it can be observed that the morphology of the particles is all flake-like, but the particle size distribution is broad as previous reports [9,11].It is clear that the particle size ranges from 4 μm to 7 μm and the thickness is about 300 nm. The huge particle size is caused by the un-homogeneous precipitation process, which can be overcome through optimizing the precipitation temperature or other conditions. Another scheme is that some flake-like materials (such as Graphene) can be used as templates to control the morphology and size distribution of particles. Those works will be done in our future work.

Besides that, XPS was used to confirm the oxidation state of the Mn atoms in the acquired $Mn(PO_3(OH))\cdot 3H_2O$. As shown in Fig. 5, the Mn $2p_{3/2}$ core level shift of the compound is at BE = 641.5 eV, which is same as the literature value of Mn(II) oxidation state of MnO [18] Therefore, it can be confirm that the oxidation state of Mn atoms in the compound is +2 and the Mn(II) centers are bridged by neutral water molecules, not by oxo or hydroxyl groups.

Based on above results, it can be concluded that the pure flake-like $Mn(PO_3(OH))\cdot 3H_2O$ crystal can be synthesized by an easy accessible method. With this method, there is no need to adjust the pH value of the solution or maintain high temperature as several former reports [18,19].

After synthesizing the flake-like $Mn(PO_3(OH))\cdot 3H_2O$ with the novel method, the crystal was then applied in the preparation of the $LiMnPO_4$/C, $LiMn_{0.5}Fe_{0.5}PO_4$/C. The corresponding XRD patterns of the compounds are plotted in Fig. 6. All diffraction peaks of two patterns can be indexed based on the orthorhombic unit cell *Pnma* and the common impurity (Li_3PO_4, $Mn_2P_2O_7$) is not found in the terminal product. It can be confirmed that using the $Mn(PO_3(OH))\cdot 3H_2O$ precursor can limit the formation of Li_3PO_4 without introducing the $Mn_2P_2O_7$. The absence of carbon peaks in the XRD patterns of all samples indicates that carbon is in an amorphous state. Compared with the XRD pattern of $LiMnPO_4$/C, the peaks of $LiMn_{0.5}Fe_{0.5}PO_4$/C clearly shifts to high diffraction angles (Inset of Fig. 6). And the corresponding lattice parameter values of $LiMn_{0.5}Fe_{0.5}PO_4$/C are also smaller than those of $LiMnPO_4$/C as shown in Table 1. It is because that ionic radii of Fe^{2+} (0.74 Å) is smaller than Mn^{2+} (0.8 Å) so that the Fe substitution results in the cell volume decrease [21]. And the results implies that Fe substitution can be

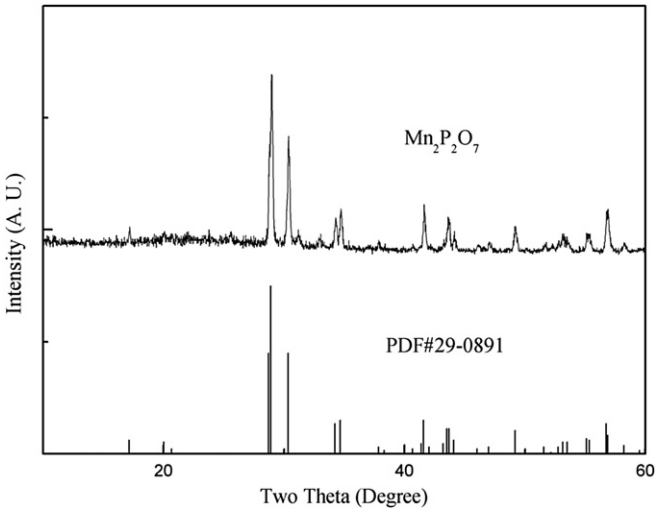

Fig. 3. XRD pattern of as-prepared $Mn_2P_2O_7$ with Cu-Kα irradiation.

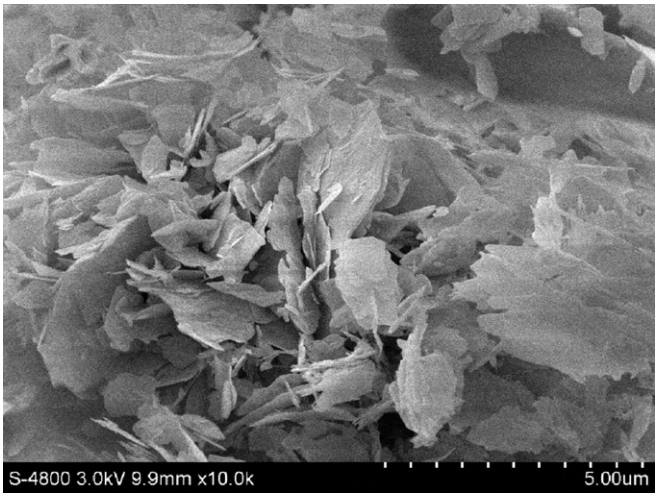

Fig. 4. SEM image of the $Mn(PO_3(OH))\cdot 3H_2O$ prepared by adding C_2H_5OH.

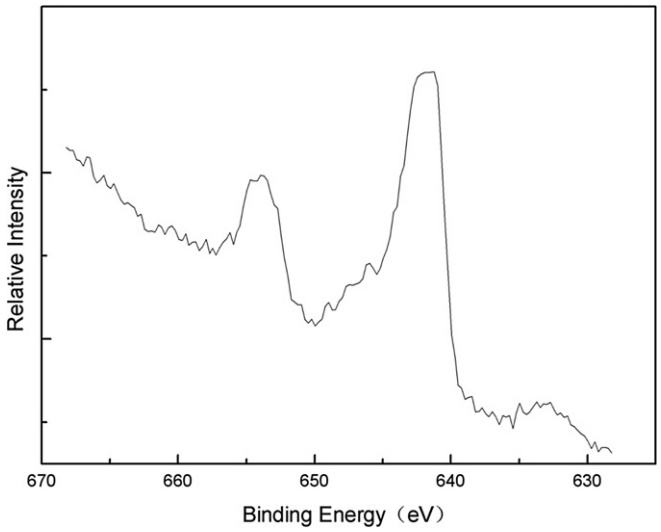

Fig. 5. Mn 2p XPS core level of the $Mn(PO_3(OH))\cdot 3H_2O$.

successfully achieved to form the $LiMn_{0.5}Fe_{0.5}PO_4$ using $Mn(PO_3(OH))\cdot 3H_2O$ precursor.

The SEM images of $LiMnPO_4$/C and $LiMn_{0.5}Fe_{0.5}PO_4$/C are shown in Fig. 7(a) and Fig. 7(b), respectively. As shown in the images, there is no significant difference between the pure and Fe-substituted samples, and the morphology and particle size of both two materials are not homogenous and different from those of $Mn(PO_3(OH))\cdot 3H_2O$ precursor due to the non-uniformity of solid-reaction among the precursors. From the magnified picture in Fig. 7(a) and (b), it can also be observed the particle size of the samples is about 0.5 μm. So the small particle size can play a positive role in improving the electrochemical performance of the terminal material for decreasing the length of the pathway for the transport of electron and ion [22]. The EDX test of the corresponding $LiMn_{0.5}Fe_{0.5}PO_4$/C was performed as shown in the Fig. 7(c), and the characteristic peaks of Mn, Fe, P, O elements are found in the EDX spectrum as expected, in which the molar ratio of the Mn:Fe:P is about 1:1:2. The results indicate the fairly uniform distribution of the elements in $LiMn_{0.5}Fe_{0.5}PO_4$ material. To observe

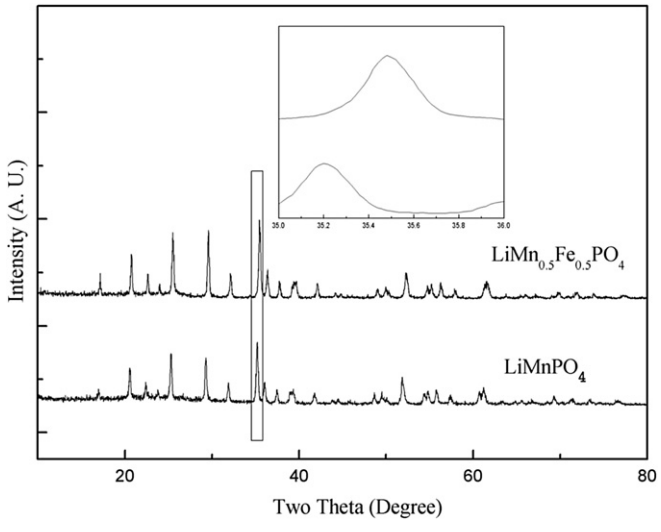

Fig. 6. XRD patterns of the $LiMnPO_4$/C, and $LiMn_{0.5}Fe_{0.5}PO_4$/C samples with Cu-Kα irradiation.

Table 1
Lattice parameters of the samples estimated by refining the XRD patterns.

Samples	a (Å)	b (Å)	c (Å)	V(Å^3)
$LiMnPO_4$	6.0977(3)	10.4428(1)	4.7396(8)	301.81
$LiMn_{0.5}Fe_{0.5}PO_4$	6.0464(5)	10.3612(4)	4.6997(5)	294.43

the morphology of the primary particle, the HRTEM of $LiMn_{0.5}Fe_{0.5}PO_4$/C was carried out. As shown in Fig. 7(d), a thin carbon layer with the thickness of 2–3 nm, which is created by sucrose, adheres to surface of the $LiMn_{0.5}Fe_{0.5}PO_4$, and the acetylene black added into the precursors also appears. Both two kinds of carbon are believed to restrain the growth of material particle effectively [14,15]. In contrast to the carbon layer and acetylene black, $LiMn_{0.5}Fe_{0.5}PO_4$ has clear lattice spacing, which is consistent with the results of XRD.

The electrochemical properties of the samples are shown in Fig. 8. The initial charge–discharge curves of the two samples at 0.05 C (7.5 mA g^{-1}) at 25 °C, which deliver discharge capacities of 69 mAh g^{-1} and 131 mAh g^{-1}, respectively, are shown in Fig. 8(a). In comparison with the $LiMnPO_4$/C, $LiMn_{0.5}Fe_{0.5}PO_4$/C has two typical potential plateaus at 4.0 V and 3.5 V vs. Li/Li^+ and also have much higher reversible capacities. It is because that the partial substitution of Fe in $LiMnPO_4$ can not only improve the conductivity of the material but also facilitate the Li^+ diffusion by lowering the large resistance for Li^+ to pass through two-phase ($MnPO_4$/$LiMnPO_4$) interface [14,15].

To confirm the improved electrochemical performances, the continuous cycling test (Fig. 8(b)) was conducted. At 0.05 C (7.5 mA g^{-1}), all samples show great cycling performance at 25 °C due to the good structural stability of olivine-structured $LiMPO_4$ (M = Mn, Fe, etc.). The disappointing capacity around 70 mAh g^{-1} of the $LiMnPO_4$/C mainly results from low intrinsic electronic conductivity and sluggish kinetics of lithium ion transport [8–11,23]. In contrast, $LiMn_{0.5}Fe_{0.5}PO_4$/C samples have obvious improved capacities, which has a capacity of 120 mAh g^{-1} after 25 cycles at 0.05 C (7.5 mA g^{-1}) maintaining its initial capacity about 91%. As shown in Fig. 8(c), the discharge capacity decreases gradually during the cycling test. But the two typical potential plateaus (at 4.0 V and 3.5 V vs. Li/Li^+) of the discharge curve at the first cycle are not as obvious as these at subsequent cycles, which is due to the surface effect and the electrochemical activation during the initial cycle. And the main capacity loss appears in the region above 3.5 V, which results from the dissolution of Mn during cycling [14,15].

The enhanced electrochemical kinetics of $LiMn_{0.5}Fe_{0.5}PO_4$/C was further demonstrated by the rate capability test. The cell was charged at 0.05 C (7.5 mA g^{-1}) to 4.5 V, held at 4.5 V until the current decreased to 1.5 mA g^{-1}, and then discharged at various rates to 2.2 V. As shown in Fig. 8(d), the reversible capacity can reach 131 mAh g^{-1} at 0.05 C, 119 mAh g^{-1} at 0.2 C, 105 mAh g^{-1} at 1 C. The capacity can be recovered at certain extent (about 94%) at 0.05 C after the rate capability test. The phenomenon of capacity loss is same as that in the cycling test. All above results demonstrate that $LiMn_{0.5}Fe_{0.5}PO_4$/C with improved electrochemical performance has been synthesized from the novel $Mn(PO_3(OH))\cdot 3H_2O$. Besides that, it is also confirmed that the electrochemical properties of the acquired $LiMn_{0.5}Fe_{0.5}PO_4$ are basically similar to those of the $LiMn_{0.5}Fe_{0.5}PO_4$ synthesized by other methods, such as, traditional solid-state, hydrothermal and sol–gel processes. But the electrochemical properties of the $LiMn_{0.5}Fe_{0.5}PO_4$ still have some advantages in certain aspects, which can be summarized as follows [8,14–16]: reducing the electrochemical inactive impurities (Li_3PO_4 etc.) that usually exist in the final product produced by traditional solid-state method, so that it can improve the electrochemical

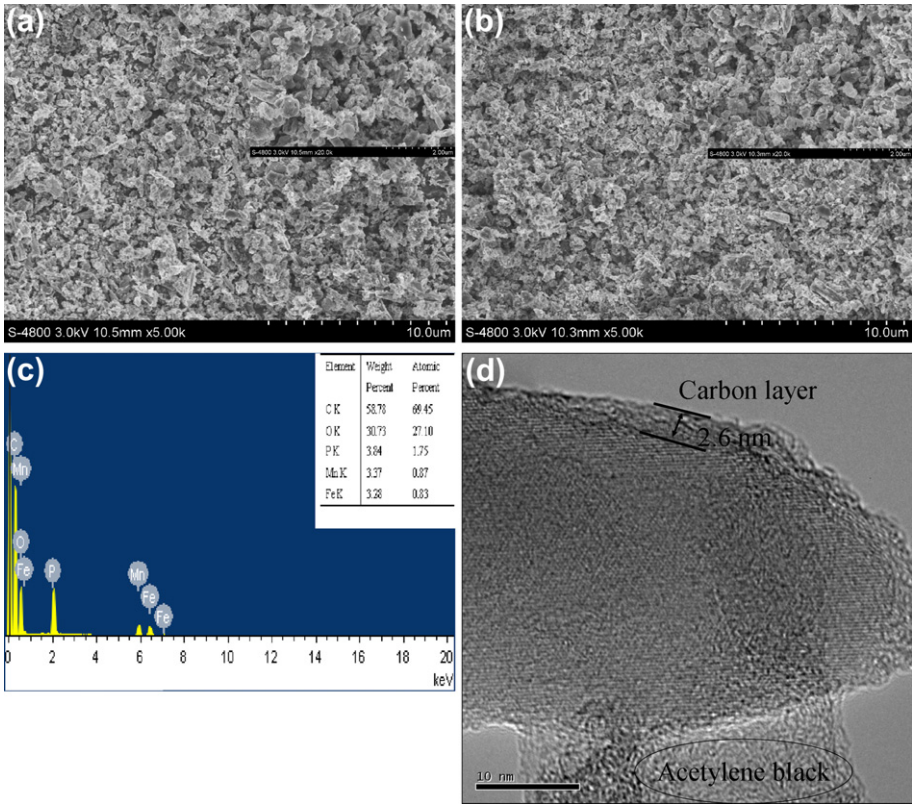

Fig. 7. (a) SEM image of the $LiMnPO_4$/C sample, (b) SEM image of the $LiMn_{0.5}Fe_{0.5}PO_4$/C sample, (c) EDS spectrum of the corresponding $LiMn_{0.5}Fe_{0.5}PO_4$/C sample and the inset is the content of different elements, (d) HRTEM image of the $LiMn_{0.5}Fe_{0.5}PO_4$/C sample.

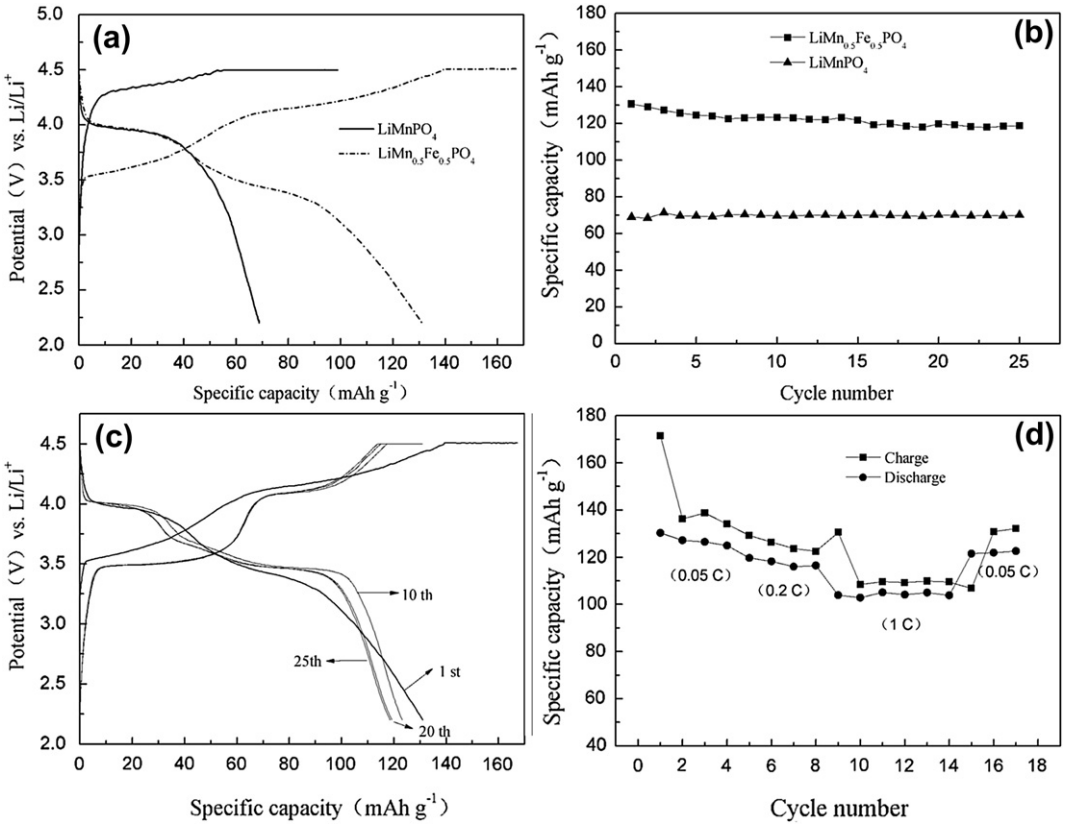

Fig. 8. (a) the first charge/discharge curves of $LiMnPO_4$/C and $LiMn_{0.5}Fe_{0.5}PO_4$/C samples at 0.05 C at 25 °C, (b) cycling performance of the three samples at 0.05 C at 25 °C, (c) resulting charge/discharge curves of $LiMn_{0.5}Fe_{0.5}PO_4$/C at 0.05 C at 25 °C, (d) rate performance of $LiMn_{0.5}Fe_{0.5}PO_4$/C by CC–CV charge mode and discharged at various rates.

performance of the final product; having potential to solve the problem of the low volumetric capacity of the products synthesized by hydrothermal, sol–gel methods.

4. Conclusions

An easy accessible, cost-effective method was successfully developed for synthesizing the pure $Mn(PO_3(OH))\cdot 3H_2O$ crystal. And the precursor prepared by the novel method was also applied in the synthesis of electrochemical active $LiMnPO_4$ and $LiMn_{0.5}Fe_{0.5}PO_4$ for the first time. From related results, it can be confirmed that the incorporation of Fe into $LiMnPO_4$ can significantly improve the electrochemical properties for improving the conductivity of the material and facilitating the Li^+ diffusion. The as-prepared $LiMn_{0.5}Fe_{0.5}PO_4$/C material exhibited an excellent reversible capacity of 131 mAh g^{-1} retaining about 91% after 25 cycles at 0.05 C. Furthermore, the sample demonstrates good rate capability that reversible capacity can reach 119 mAh g^{-1} at 0.2 C, 105 mAh g^{-1} at 1 C.

References

[1] M. Nayak, S.Y. Lee, T.Y. Tseng, Mater. Chem. Phys. 77 (2002) 34–42.
[2] S. Xiong, J. Shen, Q. Xie, Y. Gao, Q. Tang, Y. Qian, Adv. Funct. Mater. 15 (2005) 1787–1792.
[3] S. Xuan, L. Hao, W. Jiang, L. Song, Y. Hu, Z. Chen, L. Fei, T. Li, Cryst. Growth Des. 7 (2007) 430–434.
[4] J.Y. Li, S. Xiong, B. Xi, X.G. Li, Y.T. Qian, Cryst. Growth Des. 9 (2009) 4108–4115.
[5] G.A. Nazri, G. Pistoia, Lithium Batteries: Science and Technology, first ed., Kluwer, Boston, 2004.
[6] A.K. Padhi, K.S. Nanjundaswamy, J.B. Goodenough, J. Electrochem. Soc. 114 (1997) 1188.
[7] Y. Wang, Y. Yang, Y. Yang, H. Shao, Solid State Commun. 150 (2010) 81–85.
[8] J. Xiao, W. Xu, D. Choi, J.G. Zhang, J. Electrochem. Soc. 157 (2010) A142–A147.
[9] N.N. Bramnik, H. Ehrenberg, J. Alloys Compd 464 (2008) 259–264.
[10] J. Xiao, N.A. Chernova, S. Upreti, X. Chen, Z. Li, Phys. Chem. Chem. Phys. 13 (2011) 18099–18106.
[11] L. Wang, W. Sun, X. He, J. Li, C. Jiang, Int. J. Electrochem. Sci. 6 (2011) 2022–2030.
[12] A.K. Padhi, K.S. Nanjundaswamy, C. Masquelier, S. Okada, J.B. Goodenough, J. Electrochem. Soc. 144 (1997) 1188.
[13] A. Yamada, Y. Kudo, K.Y. Liu, J. Electrochem. Soc. 148 (2001) A747.
[14] K. Saravanan, V. Ramar, P. Balaya, J.J. Vittal, J. Mater. Chem. 21 (2010) 14925–14935.
[15] S.M. Oh, S.T. Myung, Y.S. Choi, K.H. Ohd, Y.K. Sun, J. Mater. Chem. 21 (2010) 19368–19374.
[16] M. Zhao, G. Huang, B. Zhang, F. Wang, X. Song, J. Power Sources 211 (2012) 202–207.
[17] Y. Cudennec, A. Riou, Y. Gerault, Acta Crystallogr. C45 (1989) 1411.
[18] C.V.K. Sharma, C.C. Chusuei, R. Clerac, T. Mo1ller, K.R. Dunbar, A. Clearfield, Inorg. Chem. 42 (2003) 8300–8308.
[19] A. Larrañaga, J.L. Mesa, J.L. Pizarro, R. Olazcuaga, F. Guillen, M.I. Arriortua, T. Rojo, J. Phys. IV France 123 (2005) 241–244.
[20] C. Delacourt, P. Poizot, M. Morcrette, J.M. Tarascon, C. Masquelier, Chem. Mater. 16 (2004) 93–99.
[21] C. Hu, H. Yi, H. Fang, B. Yang, Y. Yao, W. Ma, Y. Dai, Electrochem. Commun. 12 (2010) 1784–1787.
[22] J. Ni, Y. Kawabe, M. Morishita, M. Watada, T. Sakai, J. Power Sources 196 (2011) 8104–8109.
[23] C. Delacourt, L. Laffont, R. Bouchet, C. Wurm, J.B. Leriche, M. Morcrette, J.M. Tarascon, C. Masqueliera, J. Electrochem. Soc. 152 (2005) A913–A921.